Engineering an Anion-Binding Cavity in Antichymotrypsin Modulates the "Spring-Loaded" Serpin−Protease Interaction†

Christine M. Lukacs,‡ Harvey Rubin,§ and David W. Christianson*,‡

Departments of Chemistry and Medicine, University of Pennsylvania, Philadelphia, Pennsylvania 19104

Received September 23, 1997; Revised Manuscript Received December 9, 1997

ABSTRACT: Expressed in a kinetically trapped folding state, a serpin couples the thermodynamic driving force of a massive β-sheet rearrangement to the inhibition of a target protease. Hence, the serpin−protease interaction is the premier example of a "spring-loaded" protein−protein interaction. Amino acid substitutions in the hinge region of a serpin reactive loop can weaken the molecular spring, which converts the serpin from an inhibitor into a substrate. To probe the molecular basis of this conversion, we report the crystal structure of A349R antichymotrypsin in the reactive loop cleaved state at 2.1 Å resolution. This amino acid substitution does not block the β-sheet rearrangement despite the burial of R349 in the hydrophobic core of the cleaved serpin along with a salt-linked acetate ion. The inhibitory activity of this serpin variant is not obliterated; remarkably, its inhibitory properties are anion-dependent due to the creation of an anion-binding cavity in the cleaved serpin.

The serpin (*ser*ine *p*rotease *in*hibitor) family of proteins accounts for 10% of the total protein content of human plasma *(1)*. Various members of this family are implicated in numerous proteolytic cascades, such as those mediating inflammation, fibrinolysis, thrombolysis, and apoptosis *(1, 2)*. To date, more than 100 serpins have been identified on the basis of sequence identity with the archetypical serpin, α_1-proteinase inhibitor *(1−4)*. Despite the implication of common sequence−structure−function relationships, some of these serpins are noninhibitory, such as ovalbumin and angiotensinogen *(5−8)*. Upon incubation with a protease, these particular serpins are consumed as simple polypeptide substrates. Presumably, the function of these noninhibitory serpins diverged in order to meet alternative requirements of the cell.

The reactive loop of an inhibitory serpin is a ∼15-residue, solvent-exposed segment that is the principal determinant of protease recognition and inhibition. However, the reactive loop does not remain solvent-exposed throughout the reaction coordinate of serpin function. Upon release from a serpin−protease complex, the serpin reactive loop is cleaved and the N-terminal fragment of the cleaved bond [i.e., containing the P1 residue[1] *(9)*] inserts into β-sheet A as strand s4A—this separates the two cleaved ends by ∼70 Å (Figure 1) *(10−13)*. This massive β-sheet rearrangement is driven by the greatly increased stability of the cleaved serpin, which results from the insertion of the P3−P15 reactive loop residues in an antiparallel β-strand conformation in β-sheet A, as well as the ordering of secondary and tertiary structural elements *(14, 15)*. Hence, the β-sheet rearrangement illustrated in Figure 1 is "spring-loaded," and it is necessary but not sufficient for inhibitory activity in the serpin−protease complex *(16, 17)*.

The great structural mystery confronting the analysis of serpin function is the conformation of the serpin reactive loop in the serpin−protease complex. Recent crystal structures of uncomplexed, intact serpins *(18−22)* show that, apart from the structure of a thermostable variant of α_1-proteinase inhibitor *(22)*, the reactive loop does not adopt the so-called "canonical" conformation observed for the smaller protein inhibitors such as bovine pancreatic trypsin inhibitor or turkey ovomucoid inhibitor *(23−25)*. The serpin reactive loop must undergo significant conformational changes as the inhibitor progresses from the native state to the inhibitory state and from the inhibitory state to the cleaved state *(26, 27)*. To what degree does strand s4A insertion into β-sheet A accompany these conformational changes? Recent experiments convincingly demonstrate that, after the initial serpin−protease recognition event, the scissile bond is cleaved and strand s4A is substantially inserted into β-sheet A to form a long-lived, covalent, inhibitory complex *(28, 29)* and that this complex exhibits properties suggestive of strand insertion *(30, 31)*. Presumably, strand insertion coupled to changes in the environment of the enzyme active site must be sufficiently rapid to sequester the protease active site from solvent—this will prevent acyl-enzyme hydrolysis and premature release of the cleaved serpin *(26, 30)*.

Mutation of P14 or P12 residues of various serpins with either charged residues *(32−36)* or conformationally restrictive proline residues *(37−40)* generally transforms inhibitors

† This work was supported by grants from the National Institutes of Health, HL-51893 (to D.W.C.) and HL-50532 (to H.R.). Additionally, part of this work is based upon research conducted at the Cornell High Energy Synchrotron Source (CHESS), which is supported by the National Science Foundation under Award DMR-9311772, using the Macromolecular Diffraction at CHESS (MacCHESS) facility, which is supported by Award RR-01646 from the National Institutes of Health.

* Correspondence should be addressed to this author at the Department of Chemistry, 231 South 34th St., University of Pennsylvania, Philadelphia, PA 19104-6323: (215) 898-5714 (phone); (215) 573-2201 (fax); chris@xtal.chem.upenn.edu (e-mail).

‡ Department of Chemistry.

§ Department of Medicine.

[1] The nomenclature of Schecter and Berger is used to describe the reactive loop residues of serpins. The scissile bond in ACT, L358−S359, is notated as P1−P1′. Residues N-terminal to P1 are P2, P3, etc., and residues C-terminal to P1′ are P2′, P3′, etc.

S0006-2960(97)02359-3 CCC: $15.00 © 1998 American Chemical Society
Published on Web 02/18/1998

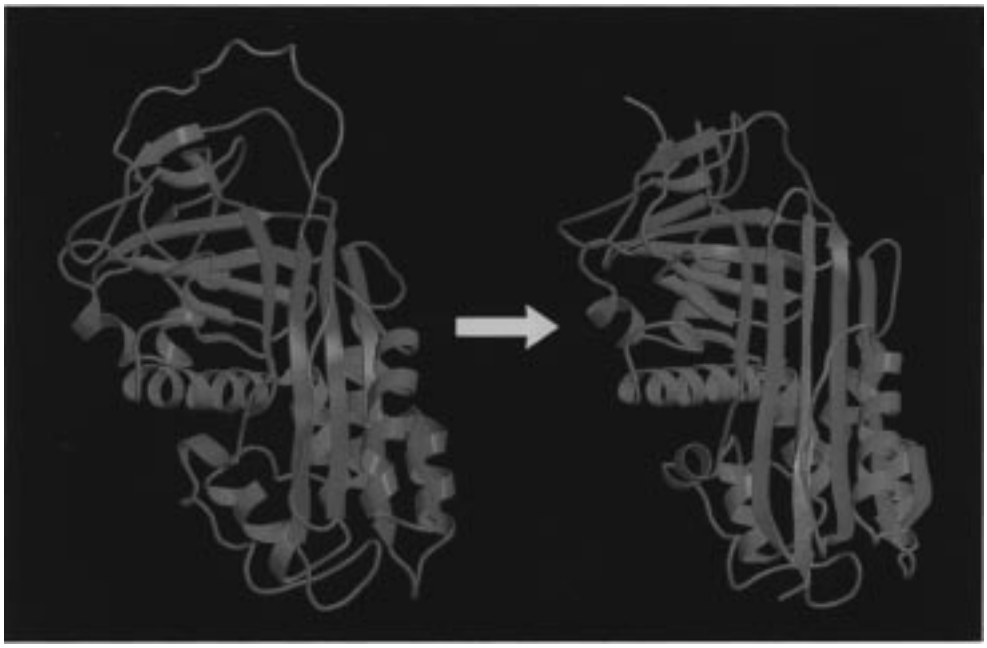

FIGURE 1: Intact → cleaved structural transition of antichymotrypsin *(11, 20)*. The "unprimed" side (i.e., containing the P15−P1 residues) of the cleaved reactive loop (red) inserts into β-sheet A as strand s4A, separating the P1 and P1′ residues by ∼70 Å. The figure was prepared with MOLSCRIPT *(64)* and Raster 3D *(65)*.

into substrates. At the P10 site, substitution of glutamic acid does not affect the inhibitory activity of α_1-antitrypsin *(35)* or plasminogen activator inhibitor 1 *(36)*, although the substitution of proline at the P10 site of α_1-antitrypsin *(41)* or plasminogen activator inhibitor 1 results in substrate behavior *(37)*. The P10−P14 residues serve as a conformational hinge for the serpin rearrangement illustrated in Figure 1; the P-even residues (P10, P12, P14) are ultimately buried in the hydrophobic protein core. Although it had been considered that radical mutations of P-even hinge residues would inhibit strand s4A insertion and therefore block inhibitory activity *(42, 43)*, these variants show increased stability upon reactive loop cleavage, suggesting at least some degree of strand s4A insertion *(33, 34, 39, 44)*. This suggestion has been verified by recent X-ray crystal structure determinations of cleaved antichymotrypsin variants with P14 and P12 arginine substitutions *(45)* and a cleaved plasminogen activator inhibitor with a proline residue substituted at the P12 position *(38)*.

To further study strand s4A insertion in hinge region variants of antichymotrypsin and to determine how P-even arginine substitutions impose a higher energetic barrier to rapid strand insertion (which compromises the spring-loaded mechanism and results in increased substrate behavior), we have prepared, characterized, and determined the X-ray crystal structure of the cleaved P10-arginine variant A349R-ACT[2] at 2.1 Å resolution. Recombinant α_1-antichymotrypsin is a 45 kDa serpin that inhibits cathepsin G and chymotrypsin. This serpin may also play a role in Alzheimer's disease *(46−49)* and the inhibition of superoxide production *(50)*. The work reported herein also complements previously determined structures of cleaved T345R-ACT (P14) at 3.1 Å resolution and A347R-ACT (P12) at 2.9 Å resolution *(45)*: we have extended the resolution of these structures to 2.9 and 2.4 Å, respectively, using cryocrystallography and synchrotron radiation.

MATERIALS AND METHODS

Site-Directed Mutagenesis, Protein Expression, and Purification. Site directed mutagenesis was carried out using plasmid pZMS-ACT *(51)* slightly modified with a longer ACT gene insert (prepared by Dr. Mei Wang). Briefly, PCR was carried out by either Vent or Taq polymerase (New England Biolabs), using synthetic primers (Children's Hospital of Pennsylvania Abramson Center Core Facility) designed to incorporate the mutation (5′-AGGGCCACAGCAGTCAAATC-3′ and 5′-TTGACTGCTGTGGCCCTAGATGCTTCTGTGCCC-3′) and to create a *Kpn*I restriction site at the COOH-terminus (5′-TTTTTGGTACCCTAGGCTTGCTTGGGAT-3′) in order to eliminate the possibility of reverse insertion. The variant gene and the original plasmid were cut with restriction enzymes *Apa*I and *Kpn*I (New England Biolabs), ligated with T4 ligase (New England Biolabs), and transformed into competent *Escherichia coli* 4830 cells. DNA sequencing (University of Pennsylvania DNA Sequencing Facility) confirmed the incorporation of the mutation and no PCR errors were detected.

Protein was expressed in *E. coli* and purified as previously described *(51)*, using Q Sepharose Fast Flow (Pharmacia Biotech) and DNA−cellulose (Sigma) in successive chromatographic purification steps. To cleave the reactive loop of A349R-ACT, 5.3 mg (∼120 nmol) of purified protein was incubated with 200 pmol of chymotrypsin (Worthington) in 1 M sodium/potassium phosphate, pH 7.0, in a volume of 15 mL at room temperature for 5 days. At this point, SDS−PAGE confirmed that cleavage was complete. The solution was heated to 70 °C for 1 h and then centrifuged to remove any denatured protein.

[2] Abbreviations: ACT, human antichymotrypsin; T345R, threonine-345 → arginine; A347R, alanine-347 → arginine; A349R, alanine-349 → arginine; PCR, polymerase chain reaction; SDS−PAGE, sodium dodecyl sulfate−polyacrylamide gel electrophoresis; SI, stoichiometry of inhibition; GuHCl, guanidine hydrochloride.

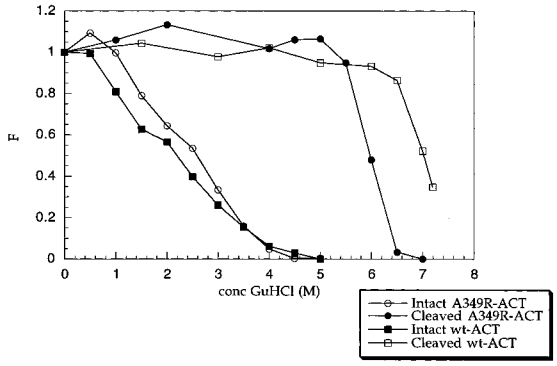

FIGURE 2: Unfolding of intact and cleaved wild-type ACT and A349R-ACT by increasing guanidine hydrochloride concentrations as monitored by changes in ellipticity (*F*) at 220 nm. The intact serpins exhibit comparable stabilities and are completely unfolded by 5.0 M GuHCl. The cleaved serpins are much more stable and do not reach their completely unfolded states until ~8.0 M GuHCl.

Determination of the Stoichiometry of Inhibition. The stoichiometry of inhibition (SI) of A349R-ACT against chymotrypsin was determined as previously described *(51)*. Briefly, chymotrypsin was titrated with increasing amounts of A349R-ACT in standard conditions (200 nM enzyme, 0.5 M NaCl, 0.1 M Tris, and 0.01% dodecyl maltoside, pH 8.0) with a 20 min incubation time (0.5 M NaCl was replaced by other salts as necessary to assess the effects of different anions on inhibitory activity). Aliquots were taken from the incubated mixture to make a 40 pM enzyme solution in 0.2 M NaCl, 0.45 M Tris, pH 8.0, and 1 mM *N*-methoxysuccinyl-Ala-Ala-Pro-Phe-*p*-nitroaniline (Sigma). Residual chymotrypsin activity was measured by following the release of *p*-nitroaniline at 410 nm.

Stability of Intact and Cleaved A349R-ACT and Native ACT. The stabilities of both the intact and cleaved forms of A349R-ACT and native ACT were measured by monitoring changes in ellipticity at 220 nm at increasing concentrations of guanidine hydrochloride (GuHCl). ACT was concentrated to 2 mg/mL in 100 mM sodium chloride and 10 mM sodium phosphate, pH 7.5. Samples of 300 μL total volume were prepared by incubating 30 μL of protein with the appropriate dilution of an 8 M GuHCl stock solution (in 100 mM sodium chloride and 10 mM sodium phosphate, pH 7.5) for 1 h. Ellipticity measurements were made on a Jasco J-600 spectropolarimeter using a 1 mm quartz cuvette. Four scans of each sample were taken from 255 to 200 nm, and the difference spectrum between each sample and the appropriate blank was calculated. Each experiment was performed at least twice (Figure 2).

Crystal Structure Determination of A349R-ACT. Crystallization of A349R-ACT was achieved by the vapor diffusion method. A hanging drop containing 4 μL of A349R-ACT (3 mg/mL in deionized water) plus 2.5 μL of precipitant buffer (14% poly(ethylene glycol) monomethyl ether 5000, 0.2 M magnesium acetate, and 0.1 M sodium citrate, pH 5.6) was equilibrated against 1 mL of the precipitant buffer in the crystallization reservoir. Large parallelepipedons (0.3 mm × 0.3 mm × 0.6 mm) appeared in 1−2 weeks and X-ray diffraction analysis indicated space group $P2_12_12_1$ with unit cell parameters $a = 71.7$ Å, $b = 78.4$ Å, and $c = 79.2$ Å. These crystals diffracted X-rays to a resolution of 2.1 Å on an R-Axis IIc image plate detector. Individual ϕ oscillation images spanning 1.0° were collected for 20 min each over a total angular range of 100°. The crystal-to-detector distance was set to 10 cm and the swing angle 2θ was set to 0°. The crystal orientation matrix was initially obtained and reflections were integrated with MOSFLM *(52)*, and data reduction was completed with CCP4 *(53)*.

The structure of A349R-ACT was initially determined and refined at 2.7 Å resolution. The atomic coordinates of cleaved recombinant A347R-ACT (which crystallizes isomorphously with cleaved A349R-ACT) less strand s4A were used to generate the initial electron density map by the difference Fourier method. After rigid-body refinement in X-PLOR *(54)*, the crystallographic *R*-factor was 0.357 (R_{free} = 0.370). After one round of positional refinement, the *R*-factor dropped to 0.297 (R_{free} = 0.370). Difference electron density maps calculated at this stage revealed strong and continuous density for all of strand s4A, including clear density for the R349 side chain buried in the protein core. The strand was built into the map using CHAIN *(55)*. The protein model was further refined by simulated annealing with molecular dynamics using X-PLOR. After the collection of 2.1 Å resolution data, an electron density peak adjacent to the buried guanidinium group of R349, which had initially been interpreted as a solvent molecule, assumed a triangular shape. This peak was subsequently modeled as an acetate ion. Due to the high quality and resolution of the diffraction data, additional residues at the N-terminus of the protein (residues G25 and L26) were visible and were built into the final model. The T85−E91 and N105−E109 loops, which had been characterized by poor electron density in all previous ACT variants studied *(45)*, were carefully refit. Electron density was not observed for the P1′−P7′ segment of the cleaved reactive loop; N-terminal sequencing of dissolved crystals of A347R-ACT showed that the protein has been further cleaved by chymotrypsin at the P3′−P4′ (L361−V362) linkage *(45)*. Fifty-seven solvent molecules were included in the final model. With the inclusion of bulk solvent parameters and the refinement of individual *B*-factors, refinement converged to a final crystallographic *R*-factor of 0.198 (R_{free} = 0.240) for 20.0−2.1 Å data with excellent stereochemistry. Data reduction and refinement statistics are recorded in Table 1. Refined coordinates have been deposited in the Brookhaven Protein Data Bank.[3]

Refinement of T345R-ACT and A347R-ACT Structures against Synchrotron Data. Crystals of T345R-ACT and A347R-ACT were grown as previously described *(45)*. Crystals were gradually transferred to a cryobuffer containing 20% 2-methyl-2,4-pentanediol, 10% poly(ethylene glycol) monomethyl ether 5000, 0.2 M magnesium acetate, and 0.1 M sodium citrate (pH 6.5). Diffraction data for T345R-ACT and A347R-ACT were collected under a stream of liquid nitrogen boil-off at ca. −153 °C at beamline A-1 at the Cornell High Energy Synchrotron Source (CHESS). Individual ϕ oscillation images spanning 1.0° were collected for 8 s each over a total angular range of 90° at a crystal-to-detector distance of 10 cm. Data were processed with DENZO and reduced with Scalepack *(56)*.

Coordinate sets for cleaved T345R-ACT and A347R-ACT were obtained from our previously reported structures refined at lower resolution (PDB entries 1CT3 and 2CAA), and these

[3] PDB accession codes: T345R-ACT, 4CAA; A347R-ACT, 3CAA; A349R-ACT, 1AS4.

Table 1: Data Collection and Refinement Statistics

	A349R-ACT	A347R-ACT	T345R-ACT
number of crystals	1	1	1
number of measured reflections	95 680	63 094	37 763
number of unique reflections	26 288	15 560	11 269
maximum resolution (Å)	2.10	2.40	2.90
completeness of data (%)	98.7	83.7	95.9
R_{merge}[a]	0.066	0.101	0.085
number of reflections used in refinement	25 256	14 821	9 882
number of protein atoms	2947	2941	2935
number of solvent molecules	57	47	0
crystallographic *R*-factor[b]	0.198	0.189	0.199
R_{free}[c]	0.240	0.280	0.284
RMS deviation from ideal bond lengths (Å)	0.006	0.022	0.01
RMS deviation from ideal bond angles (deg)	1.3	2.1	1.6
RMS deviation from ideal dihedral angles (deg)	24.5	25.5	24.0
RMS deviation from ideal improper dihedral angles (deg)	1.1	1.9	1.3

[a] R_{merge} for replicate reflections, $R = \sum|I_{hi} - \langle I_h\rangle|/\sum\langle I_h\rangle$; I_{hi} = intensity measured for reflection $\boldsymbol{h}$ in data set i, $\langle I_h\rangle$ = average intensity for reflection $\boldsymbol{h}$ calculated from replicate data. [b] Crystallographic *R* factor, $R = \sum||F_o| - |F_c||/\sum|F_o|$; $|F_o|$ and $|F_c|$ are the observed and calculated structure factor amplitudes, respectively, and the summation is taken over all reflections. [c] Free *R* factor, $R = \sum||F_o| - |F_c||/\sum|F_o|$; $|F_o|$ and $|F_c|$ are the observed and calculated structure factor amplitudes, respectively, and the summation is taken over all reflections in a test set of 4−5% of unique reflections omitted from refinement.

structures were refined against the higher resolution synchrotron data. Refinement of cleaved T345R-ACT converged to a final crystallographic *R*-factor of 0.199 (R_{free} = 0.284) for 8.0−2.9 Å data with excellent stereochemistry. Refinement of cleaved A347R-ACT converged to a final crystallographic *R*-factor of 0.189 (R_{free} = 0.280) for 20.0−2.4 Å data using a bulk solvent correction and with the inclusion of 47 solvent molecules. Data reduction and refinement statistics are recorded in Table 1. Both structures were generally similar to those previously reported at lower resolution *(45)*. Updated coordinate sets have been deposited in the Brookhaven Protein Data Bank.[3]

RESULTS

Structure and Function of A349R-ACT. Denaturation of intact and cleaved A349R-ACT by guanidine hydrochloride reveals that the cleaved form is more stable than the intact form of the variant, and the cleaved form of the variant is only slightly less stable than the cleaved form of wild-type ACT (Figure 2). These results imply that A349R-ACT undergoes the spring-loaded conformational transition illustrated in Figure 1 despite the radical A349R substitution at the P10 position. Given that cleaved A349R-ACT is more stable than cleaved A347R-ACT *(45)*, it appears that the serpin better accommodates radical amino acid substitutions at P-even sites further away from the critical hinge region of the reactive loop.

The crystal structure of A349R-ACT reveals full strand s4A insertion with an intact β-sheet A hydrogen-bond network (Figure 3). This results in the burial of the R349 side chain, along with an acetate counterion, in the hydrophobic core of the protein (Figure 4). One guanidinium nitrogen of R349 is within hydrogen-bonding distance (2.9 Å, but poorly oriented) to the backbone carbonyl oxygen of V337, which is part of neighboring strand s5A of β-sheet A. Another guanidinium nitrogen donates a hydrogen bond (3.1 Å) to the backbone carbonyl oxygen of F52. The acetate oxygens make a double salt link with the R349 guanidinium group, with N···O separations of 2.9 and 3.0 Å. One acetate oxygen is also within hydrogen-bonding distance (2.7 Å) to the Oγ atom of S386 and the backbone NH group of M385 (3.0 Å, but poorly oriented).

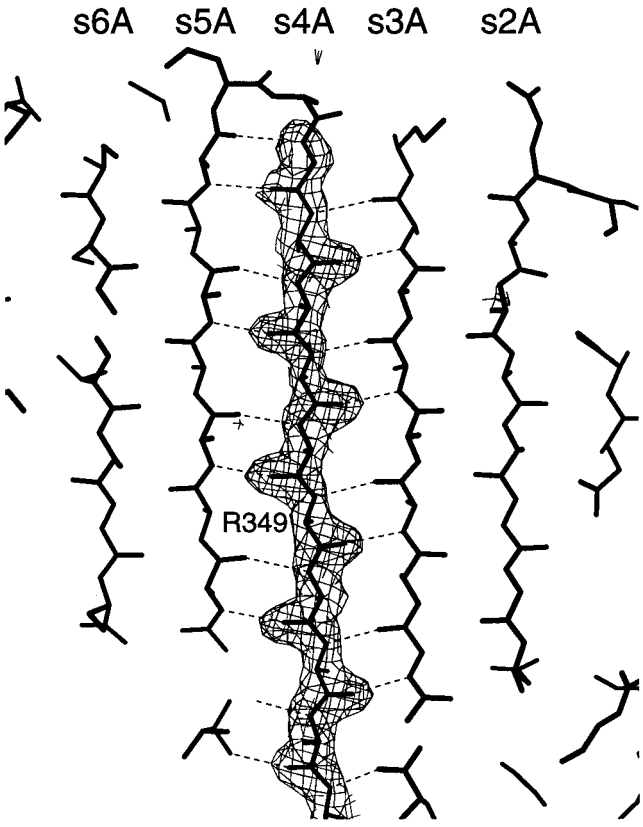

FIGURE 3: Omit map contoured at 2.5σ showing β-sheet A of cleaved A349R-ACT; strand s4A was omitted from the structure factor calculation. Refined atomic coordinates are superimposed on the map, and the Cα atom of R349 is indicated. β-Sheet hydrogen-bond interactions are indicated by dashed lines; note that antiparallel β-sheet hydrogen bonds between strand s4A and strands s3A and s5A are maintained despite the radical A349R amino acid substitution. The figure was generated with MOLSCRIPT *(64)*.

It is not surprising that the residues neighboring the radical alanine → arginine substitution in cleaved A349R-ACT move to accommodate the additional steric bulk of R349 (Figure 5). The side chain of I51 rotates ~170° to accommodate the arginine, and the side chain of S386 rotates ~125° toward the acetate ion in order to donate a hydrogen bond. The most dramatic conformational change accommodating the

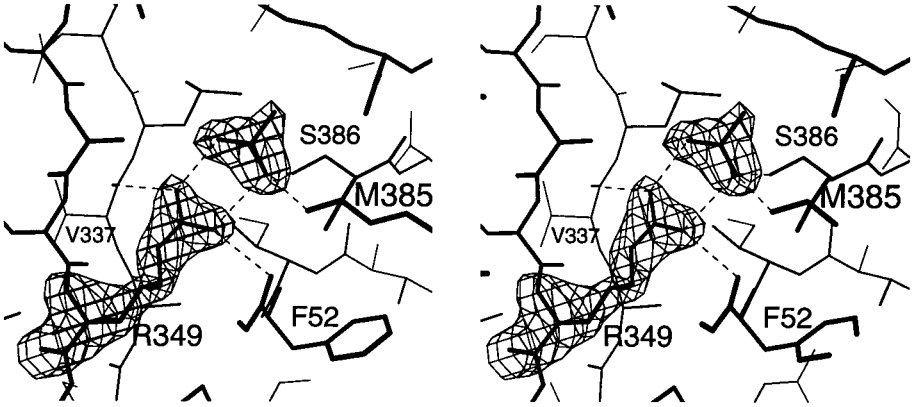

FIGURE 4: Omit map contoured at 4σ showing the buried R349−acetate ion pair in the hydrophobic core of the protein. The guanidinium group of R349 makes poorly oriented hydrogen-bond interactions with the backbone carbonyl oxygen atoms of V337 and F52. The buried acetate ion not only compensates the charge of the R349 guanidinium group but also makes hydrogen bond interactions with the Oγ of S386 and the backbone NH group of M385. Hydrogen-bond interactions are indicated by dashed lines. The figure was generated with MOLSCRIPT *(64)*.

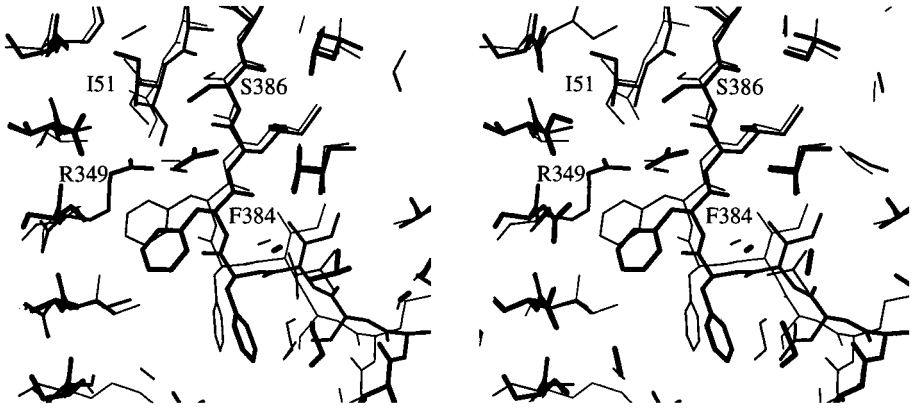

FIGURE 5: Stereoview of superimposed β-sheets A of cleaved A349R-ACT (thick bonds) and cleaved native ACT *(11)* (thin bonds). β-Sheet A is going into the page on the left side of the figure. The main-chain atoms of β-sheet A do not undergo substantial conformational changes. Instead, residues surrounding the radical A349R substitution adjust in order to accommodate the increased steric bulk.

R349 side chain is a ~1.5 Å movement and ~22° rotation of F384, which results in a significant movement of strand s5B containing this residue and adjacent loop segment V375−N381. As observed in the structure of cleaved A347R-ACT, β-sheet B serves as a "shock absorber" to help accommodate the burial of the substituted arginine residue in β-sheet A *(45)*. In fact, F384 plays a critical role in the shock absorber function of β-sheet B. Specifically, compare the structures of A347R-ACT and A349R-ACT (Figure 6)—the guanidinium group of the substituted arginine residue and the side chain of F384 occupy reversed, complementary positions in the two variants. Residue F383 also moves slightly (along with the corresponding backbone atoms) to facilitate the conformational change of F384.

The burial of the acetate ion in the hydrophobic core of A349R-ACT is rather surprising, especially since the protein was not exposed to acetate prior to crystallization: the serpin was cleaved, and strand s4A was fully inserted into β-sheet A, prior to its encounter with the 0.2 M magnesium acetate contained in the precipitant buffer. Possibly, cleaved A349R-ACT initially contains a small, empty cavity adjacent to the R349 guanidinium group, and upon incubation with acetate the small anion can penetrate ~8 Å beneath the protein surface to occupy this cavity. Alternatively, perhaps acetate exchanges with some other ligand already buried in the cavity, e.g., chloride anion or a water molecule. Notably, exchange of small buried ligands in a crystalline protein is

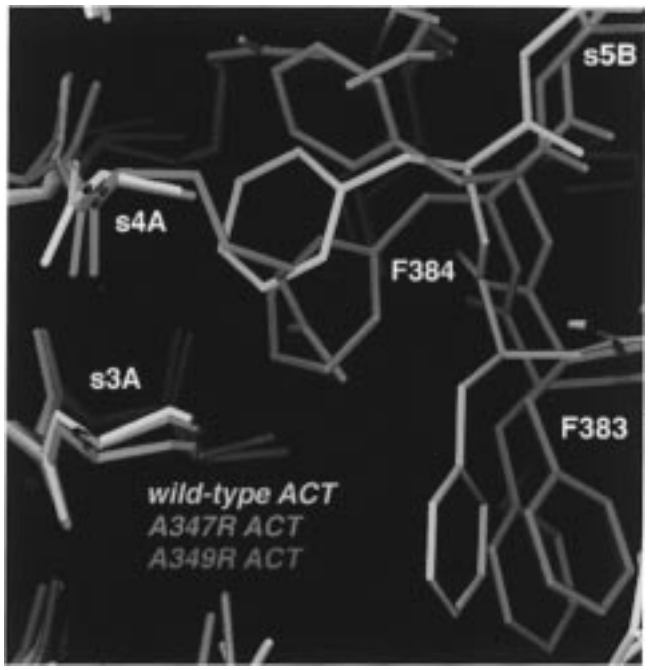

FIGURE 6: Superimposition of β-sheets A of native ACT *(11)* (yellow), A347R-ACT (blue), and A349R-ACT (pink). In A347R-ACT and A349R-ACT, the guanidinium group of the engineered arginine residue and the side chain of F384 occupy reversed, complementary positions. The figure was prepared with O *(66)*.

Table 2: Anion Dependence in the Stoichiometry of Inhibition of A349R-ACT

anion	concentration (mM)	stoichiometry of inhibition	
		wild type	A349R
Cl^-	500	1	5 ± 1
Cl^-	200	1	6.9
CH_3COO^-	500	1	7.5
CH_3COO^-	200	1	12 ± 2
Br^-	500	1	5
F^-	200	1	15 ± 0.5
I^-	500	1.3	10 ± 2
I^-	200	1.1	8.5

not without precedent. Eriksson and colleagues *(57)* describe the crystal structure of a T4 lysozyme engineered with an internal cavity 7 Å beneath the surface of the protein. Crystals of this variant equilibrated with benzene vapor yield an X-ray structure showing that benzene can penetrate the protein surface, bind in the engineered cavity, and stabilize the protein. The driving force for acetate binding in the anion-binding cavity of A349R-ACT, with resultant stabilization of the cleaved serpin, is presumably sufficient to overcome the structural barriers to protein surface penetration. The creation of a specific anion-binding cavity therefore accounts for the anion-dependent inhibitory activity of this serpin variant.

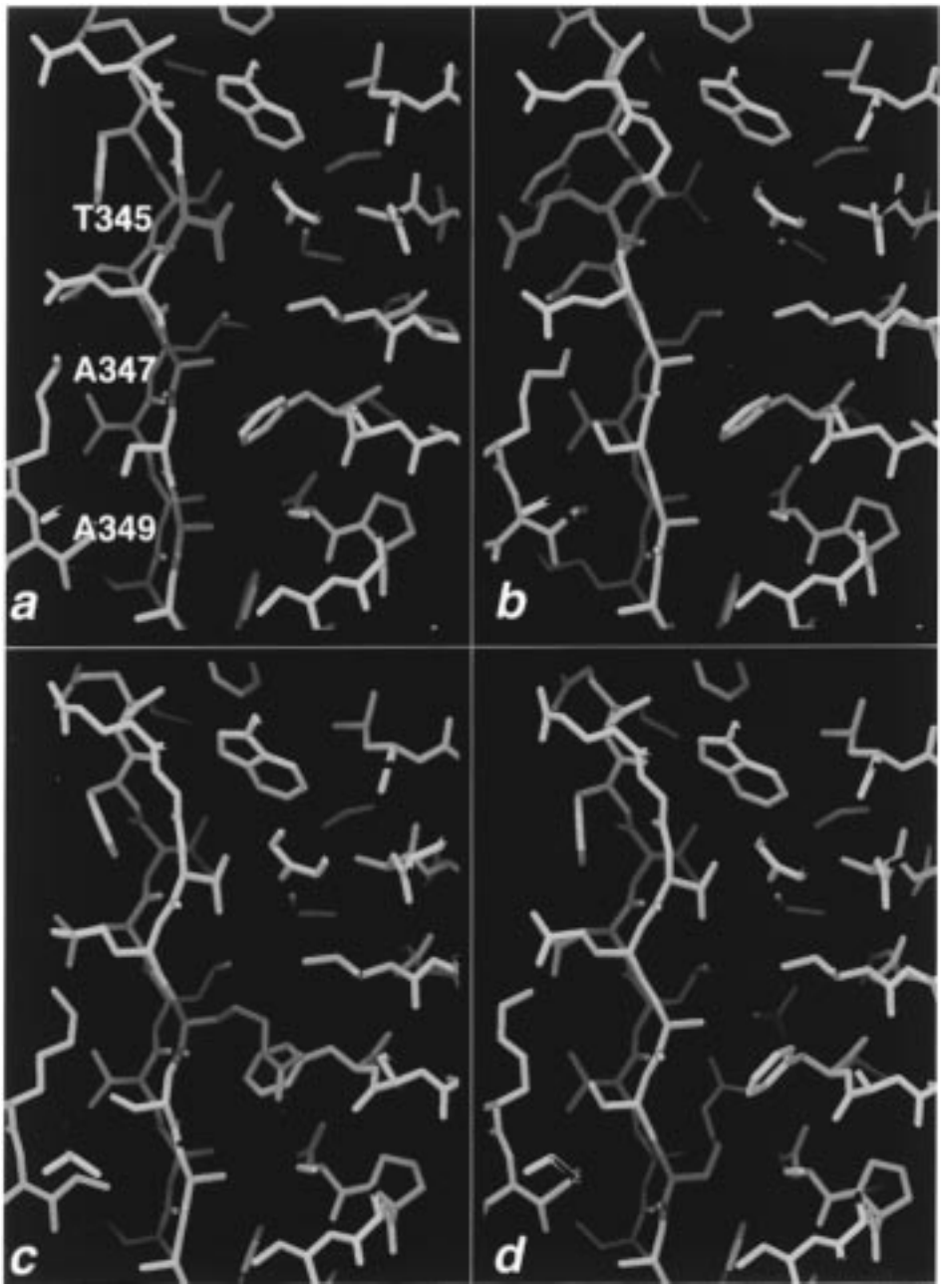

FIGURE 7: Structures of cleaved wild-type ACT (a), P14 T345R-ACT (b), P12 A347R-ACT (c), and P10 A349R-ACT (d). The P14 residue is in green, the P12 residue is in blue, and the P10 residue is in pink. Comparison of the structures reveals that the cleaved serpin accommodates hinge region arginine substitutions in three different ways: T345R-ACT (b) distorts the backbone of strand s4A so that R345 is solvent-exposed; A347R-ACT (c) buries R347 in the hydrophobic protein core with no compensating hydrogen bonds, leaving the overall strand s4A conformation undistorted; and A349R-ACT (d) buries R349 in the hydrophobic protein core along with a compensating acetate counterion, leaving the overall strand s4A conformation undistorted. The figure was prepared with O *(66)*.

The stoichiometry of inhibition of A349R-ACT ranges from 5 to 15 depending upon the type and concentration of anions in the buffer (Table 2): the greater the anion concentration, the greater the inhibitory activity. These data indicate that the inhibitory activity of this variant is only slightly compromised, which is consistent with trends observed for other s4A variants of serpins: the further away the P-even arginine substitution is made from the critical T345 hinge region, the less it affects inhibitory activity *(33*−*36, 58*). Anion-dependent inhibitory activity is not observed for wild-type ACT, so anion modulation is solely a consequence of the A349R-ACT substitution. In comparison, both A347R-ACT and T345R-ACT are chymotrypsin substrates *(31, 45, 59*).

Structures of Cleaved T345R-ACT and A347R-ACT. We have previously described the X-ray crystal structures of these cleaved P14 and P12 arginine variants of ACT *(45*). Now, we have extended the resolution of these crystal structures in order to improve the final models resulting from crystallographic refinement. No major structural differences are observed between the previously reported structures and the current structures refined at higher resolution. However, the higher resolution electron density maps clarify certain regions of each structure. For example, in the structure of T345R-ACT refined at 3.1 Å resolution, there was no observable electron density for the R345 side chain beyond the Cβ atom; in the currently refined structure at 2.9 Å resolution, electron density is observable for the entire R345 side chain. Extension of the structure of A347R-ACT from 2.9 to 2.4 Å resolution allows for the interpretation of well-defined water molecules. Importantly, no solvent molecules are buried along with the R347 guanidinium group in the hydrophobic protein core of this variant, consistent with our previous conclusions *(45*).

DISCUSSION

It is instructive to compare the three different modes by which antichymotrypsin accommodates radical arginine substitutions at the P14, P12, and P10 positions of the cleaved reactive loop: each structure illustrates novel serpin structure−stability relationships that modulate the spring-loaded serpin−protease interaction (Figure 7). Due to the absolute requirement of serpin conformational change for inhibitory activity against a target protease, these structure−stability relationships impact serpin function due to slower strand s4A insertion rates. Slower strand insertion rates will contribute to the conversion of a serpin from a protease inhibitor into a protease substrate *(26, 33, 34*).

In T345R-ACT, the arginine substitution occurs at the first residue to nucleate antiparallel β-sheet hydrogen bonding between strand s4A and adjacent strands s3A and s5A. Burial of the charged side chain in the protein core is avoided by twisting the backbone of the E343−E346 segment, which leaves the R345 side chain fully exposed to solvent *(45*). However, this deformation is made with a severe cost to overall protein stability: the conformation of R345 adopts an unfavorable conformation, and a 61 Å^3 cavity is introduced into the protein core due to the lack of a buried side chain at position 345. We propose that with R345 adopting an unfavorable conformation in the cleaved serpin, and with the resulting empty cavity in the protein core [cavities are known to destabilize proteins *(57, 60, 61*)], strand s4A insertion is much slower in the variant than in the wild-type serpin. This results in substrate behavior for this variant *(59*).

In A347R-ACT, full strand s4A insertion is observed despite the complete burial of the R347 side chain in the hydrophobic protein core *(45*). Apparently, the driving force for strand insertion is sufficient to overcome the barriers confronting the burial of the bulky R347 side chain. In this variant, the structural basis of destabilization appears to be the required conformational changes of residues surrounding the buried R347 side chain, which results in substantial packing defects. Furthermore, the R347 side chain is not stabilized with any hydrogen bonds to protein or nonprotein atoms; however, there are nearby aromatic groups that, although not optimally oriented, might compensate the positive charge of the R347 side chain with their electronic quadrupoles *(62, 63*). Alternatively, it is possible that R347 is uncharged in this environment, which would imply a pK_a depressed by about 6 units *(45*). We propose that with either of these alternatives, strand s4A insertion is much slower than in the wild-type serpin, which results in substrate behavior.

Finally, in A349R-ACT, full strand insertion is observed (this was the implication of a low SI value). However, the environment of the buried P10 arginine residue is not as hydrophobic as that surrounding the buried P12 arginine of A347R-ACT: the P10 arginine of A349R-ACT makes a number of interactions with protein atoms as well as with a compensating, buried acetate ion. The energetic cost of burying the arginine at P10 is not as large as for the P14 and P12 variants. Strand s4A insertion to the P10 position is thus achieved more rapidly, giving rise to substantial residual inhibitory activity. However, it is important to note that this variant is not a perfect inhibitor. Even with the optimal selection of anion and concentration in the assay buffer (Table 2), for every A349R-ACT that complexes to chymotrypsin, ~5 are cleaved. Thus, there is still a modest barrier to rapid strand s4A insertion in this variant. Nevertheless, the retention of appreciable inhibitory activity in A349R-ACT suggests that slow insertion of the remaining P9−P3 residues will have minimal effect on the inhibitory function of a serpin. That the insertion kinetics of the P14−P10 segment of A349R-ACT (and thus serpin−protease association) are modulated by an engineered anion-binding pocket is a unique property of spring-loaded protein−protein interactions.

ACKNOWLEDGMENT

We thank Dr. Mei Wang, Dr. Michael Plotnick, Dr. Kui Xu, and David Favor for their technical advice and helpful suggestions. Additionally, we thank Dr. Amos B. Smith III for access to the spectropolarimeter.

REFERENCES

1. Travis, J., and Salvesen, G. S. (1983) *Annu. Rev. Biochem. 52,* 655−709.
2. Gettins, P. G. W., Patston, P. A., and Olson, S. T. (1996) *Serpins: Structure, Function, and Biology*, R. G. Landes Company, Austin, TX.
3. Gettins, P., Patston, P. A., and Schapira, M. (1992) *Hematol./ Oncol. Clin. North Am. 6,* 1393−1408.

4. Stein, P. E., and Carrell, R. W. (1995) *Nat. Struct. Biol. 2,* 96−113.
5. Doolittle, R. F. (1983) *Science 222,* 417−419.
6. Wright, H. T. (1984) *J. Biol. Chem. 259,* 14335−14336.
7. Mast, A., Enghild, J., Pizzo, S., and Salveson, G. (1991) *Biochemistry 30,* 1723−1730.
8. Remold-O'Donnell, E. (1993) *FEBS Lett. 315,* 105−108.
9. Schecter, I., and Berger, A. (1967) *Biochem. Biophys. Res. Commun. 27,* 157−162.
10. Löbermann, H., Tokuoka, R., Deisenhofer, J., and Huber, R. (1984) *J. Mol. Biol. 177,* 531−556.
11. Baumann, U., Huber, R., Bode, W., Grosse, D., Lesjak, M., and Laurell, C. B. (1991) *J. Mol. Biol. 218,* 595−606.
12. Baumann, U., Bode, W., Huber, R., Travis, J., and Potempa, J. (1992) *J. Mol. Biol. 226,* 1207−1218.
13. Mourey, L., Samama, J.-P., Delarue, M., Petitou, M., Choay, J., and Moras, D. (1993) *J. Mol. Biol. 232,* 223−241.
14. Bruch, M., Weiss, V., and Engel, J. (1988) *J. Biol. Chem. 263,* 16626−16630.
15. Gettins, P., and Harten, B. (1988) *Biochemistry 27,* 3634−3639.
16. Schulze, A. J., Baumann, U., Knof, S., Jaeger, E., Huber, R., and Laurell, C.-B. (1990) *Eur. J. Biochem. 194,* 51−56.
17. Carrell, R. W., Evans, D. L., and Stein, P. E. (1991) *Nature 353,* 576−578.
18. Carrell, R. W., Stein, P. E., Fermi, G., and Wardell, M. R. (1994) *Structure 2,* 257−270.
19. Schreuder, H. A., de Boer, B., Dijkema, R., Mulders, J., Theunissen, H. J. M., Grootenhuis, P. D. J., and Hol, W. G. J. (1994) *Nat. Struct. Biol. 1,* 48−54.
20. Wei, A., Rubin, H., Cooperman, B. S., and Christianson, D. W. (1994) *Struct. Biol. 1,* 251−258.
21. Song, H. K., Lee, K. N., Kwon, K.-S., Yu, M.-H., and Suh, S. W. (1995) *FEBS Lett. 377,* 150−154.
22. Elliott, P. R., Lomas, D. A., Carrell, R. W., and Abrahams, J. P. (1996) *Nat. Struct. Biol. 3,* 676−681.
23. Fujinaga, M., Sielecki, A. R., Read, R. J., Ardelt, W., Laskowski, M. J., and James, M. N. G. (1987) *J. Mol. Biol. 195,* 397−418.
24. Bode, W., and Huber, R. (1992) *Eur. J. Biochem. 204,* 433−451.
25. Frigerio, F., Coda, A., Pugliese, L., Lionetti, C., Menegatti, E., Amiconi, G., Schnebli, H. P., Ascenzi, P., and Bolognesi, M. (1992) *J. Mol. Biol. 225,* 107−123.
26. Wright, H. T., and Scarsdale, J. N. (1995) *Proteins: Struct., Funct., Genet. 22,* 210−225.
27. Whisstock, J., Lesk, A. M., and Carrell, R. (1996) *Proteins: Struct., Funct., Genet. 26,* 288−303.
28. Lawrence, D. A., Ginsburg, D., Day, D. E., Berkenpas, M. B., Verhamme, I. M., Kvassman, J.-O., and Shore, J. D. (1995) *J. Biol. Chem. 270,* 25309−25312.
29. Wilczynska, M., Fa, M., Ohlsson, P.-I., and Ny, T. (1995) *J. Biol. Chem. 270,* 29652−29655.
30. Plotnick, M. I., Mayne, L., Schechter, N. M., and Rubin, H. (1996) *Biochemistry 35,* 7586−7590.
31. Zhong, Q. (1996) Ph.D. Thesis, University of Pennsylvania, Philadelphia, PA.
32. Davis, A. E., Aulak, K., Parad, R. B., Stecklein, H. P., Eldering, E., Hack, C. E., Kramer, J., Strunk, R. C., Bissler, J., and Rosen, F. S. (1992) *Nat. Genet. 1,* 354−358.
33. Hood, D. B., Huntington, J. A., and Gettins, P. G. W. (1994) *Biochemistry 33,* 8538−8547.
34. Lawrence, D. A., Olson, S. T., Palaniappan, S., and Ginsburg, D. (1994) *J. Biol. Chem. 269,* 27657−27662.
35. Hopkins, P. C. R., and Stone, S. R. (1995) *Biochemistry 34,* 15872−15879.
36. Tucker, H. M., Mottonen, J., Goldsmith, E. J., and Gerard, R. D. (1995) *Nat. Struct. Biol. 2,* 442−445.
37. Audenaert, A.-M., Knockaert, I., Collen, D., and Declerck, P. J. (1994) *J. Biol. Chem. 269,* 19559−19564.
38. Aertgeerts, K., De Bondt, H. L., De Ranter, C. J., and Declerck, P. J. (1995) *Nat. Struct. Biol. 2,* 891−897.
39. Sancho, E., Declerck, P. J., Price, N. C., Kelly, S. M., and Booth, N. A. (1995) *Biochemistry 34,* 1064−1069.
40. Gils, A., Knockaert, I., and Declerck, P. J. (1996) *Biochemistry 35,* 7474−7481.
41. Hopkins, P. C. R., Carrell, R. W., and Stone, S. R. (1993) *Biochemistry 32,* 7650−7657.
42. Schulze, A. J., Huber, R., Degryse, E., Speck, D., and Bischoff, R. (1991) *Eur. J. Biochem. 202,* 1147−1155.
43. Carrell, R. W., and Stein, P. E. (1996) *Biol. Chem. Hoppe-Seyler 377,* 1−17.
44. Wright, H. T., and Blajchman, M. A. (1994) *FEBS Lett. 348,* 14−16.
45. Lukacs, C. M., Zhong, J. Q., Plotnick, M. I., Rubin, H., Cooperman, B. S., and Christianson, D. W. (1996) *Nat. Struct. Biol. 3,* 888−893.
46. Abraham, C. R., Selkoe, D. J., and Potter, H. (1988) *Cell 52,* 487−501.
47. Potter, H., Nelson, R. B., Das, S., Siman, R., Kayyali, U. S., and Dressler, D. (1992) *Ann. N.Y. Acad. Sci. 674,* 161−173.
48. Janciauskiene, S., Eriksson, S., and Wright, H. T. (1996) *Nat. Struct. Biol. 3,* 668−670.
49. Lukacs, C. M., and Christianson, D. W. (1996) *Proteins: Struct., Funct., Genet. 25,* 420−424.
50. Kilpatrick, L., Johnson, J. L., Nickbarg, E. B., Wang, Z.-M., Clifford, T. F., Banach, M., Cooperman, B. S., Douglas, S. D., and Rubin, H. (1991) *J. Immun. 146,* 2388−2393.
51. Rubin, H., Wang, Z., Nickbarg, E. B., McLarney, S., Naidoo, N., Schoenberger, O. L., Johnson, J. J., and Cooperman, B. S. (1990) *J. Biol. Chem. 265,* 1199−1207.
52. Leslie, A. G. W. (1992) *Joint CCP4 and ESF-EACMB Newsletter on Protein Crystallography*, Daresbury Laboratory, Warrington, U.K.
53. Collaborative Computing Project, Number 4 (1994) *Acta Crystallogr. D50,* 760−763.
54. Brünger, A. T. (1992) *X-PLOR (v. 3.1)—A System for X-ray Crystallography and NMR*, Yale University Press: New Haven, CT.
55. Sack, J. S. (1988) *J. Mol. Graphics 6,* 224−225.
56. Otwinowski, Z. (1993) *Oscillation Data Reduction Program*, CCP4 Study Weekend (Sawyer, L., Isaacs, N., and Bailey, S., Eds.) pp 56−62, SERC Daresbury, Daresbury, U.K.
57. Eriksson, A. E., Baase, W. A., Wozniak, J. A., and Matthews, B. W. (1992) *Nature 355,* 371−373.
58. Skriver, K., Wikoff, W. R., Patston, P. A., Tausk, F., Schapira, M., Kaplan, A. P., and Bock, S. C. (1991) *J. Biol. Chem. 266,* 9216−9221.
59. Katz, D. S., Wei, A., Zhong, Q., Rubin, H., Cooperman, B. S., and Christianson, D. W. (1993) *Biochem. Biophys. Res. Commun. 196,* 752−757.
60. Hubbard, S. J., Gross, K.-H., and Argos, P. (1994) *Protein Eng. 7,* 613−626.
61. Williams, M. A., Goodfellow, J. M., and Thornton, J. M. (1994) *Protein Sci. 3,* 1224−1235.
62. Burley, S. K., and Petsko, G. A. (1986) *FEBS Lett. 203,* 139−143.
63. Flocco, M. M., and Mowbray, S. L. (1994) *J. Mol. Biol. 235,* 709−717.
64. Kraulis, P. J. (1991) *J. Appl. Crystallogr. 24,* 946−950.
65. Merrit, E. A., and Murphy, M. E. P. (1994) *Acta Crystallogr. D50,* 869−873.
66. Jones, T. A., Zou, J.-Y., Cowan, S. W., and Kjeldgaard, M. (1991) *Acta Crystallogr. A47,* 110−119.

BI972359E